A CFD INVESTIGATION OF FLOW-FIELD GEOMETRY'S EFFECT ON A TRANSIENT PERFORMANCE OF AUTOMOTIVE POLYMER ELECTROLYTE MEMBRANE FUEL CELL

ABSTRACT

A three-dimensional, multi-species, multi-phase PEM fuel cell model was developed in order to investigate the effect of the flow-field geometry on the steady-state and transient performances of the cell under an automotive operation. The two most commonly used designs, parallel and single-serpentine flow-fields, were selected as they offer distinctive species transport modes of diffusion-dominant and convection-dominant flows in the porous layers, respectively. It was found that this difference in flow mode significantly effects membrane hydration, the key parameter in determining a successful operation. In a steady run, a serpentine flow-field increased the averaged current density under the wet condition due to superior water removal but this had a negative effect on the cell in the way that it caused membrane dry-out if dry reactant gases were used. The transient operation, on the other hand, seemed to favour the combination of a serpentine flow-field and dry reactant gases as it helped in the removal of product water and speeded up the transport of reacting species to the reactive site to find equilibrium at the new state with minimum time delay and current overshoot or undershoot which is the most important aspect of a dynamic system.

INTRODUCTION

A polymer electrolyte membrane (PEM) fuel cell, among various technologies, is regarded as one of the most promising technologies for clean and efficient power generation in the near future. Due to its high power and energy densities that allow for compact and light-weight systems compared to energy-storage based systems such as batteries, a PEMFC is also favoured by automotive engineers over batteries from an all-electric vehicle or hybrid-electric vehicle design perspective. The low operating temperature at 60-100 °C offers a great advantage in which it allows for a quick start-up and fast transient response comparable to that of batteries or even traditional internal combustion engines. A comprehensive review on polymer electrolyte membrane fuel cells can be found in a review article by Wang et al. [1]

Among various components, a bi-polar plate (or flow-field plate), where channels are etched on to provide the passages for reactant gases to flow, is considered a very important component that plays an important role in the commercialisation of PEM fuel cell and it costs approximately 60% and 30% of the total weight and cost of a single cell, respectively. An effective flow-field will help promote good and uniform species transport into the catalyst layers where the electrochemical reactions take place resulting in uniform current density distribution and guarantees minimum thermal stress in the membrane which is the most fragile element. From this perspective, a thorough understanding of the effect of flow-field design on the performance of a PEMFC is needed to speed up the commercialisation of such a technology.

The numerical study of PEM fuel cell was greatly inspired by the works of Springer et al. [2] and Bernadi et al. [3-4] published in 1991 in which they proposed the mathematical models of important elements representing a working PEM fuel cell. Though all components were not included in the models and they were 1-dimensional in nature, they served as the stepping-stone to many, more complete and multi-dimensional PEMFC models that followed. One remarkable work was published by Gurau et al. [5] in which he utilised a single-domain approach in the development of his 2-dimensional model so that all components shared the same diffusion-convection transport equations for each dependent variable allowing computational fluid dynamics (CFD) technique to be used in PEMFC modelling for the first time after it has been deployed in previous works in electrochemical systems [6-7]. The mass transport aspect of different flow-field design and its effect on the performance of a PEMFC have been revealed by many studies [8-21] through the use of computational fuel cell dynamics (CFCD).

As pointed out from the previous work of Choopanya and Yang [22], the transient response of an automotive PEMFC is of paramount importance and it should receive more attention from the researchers and engineers. However, most of the attention is focused on a control standpoint in which they seek to proposed the best control strategy or operating condition for the cell [23-29]. Additionally, these studies are often regarded as system-level in which the fundamental effect of cell-level parameters such as flow-field geometries or patterns, which are the major contributors to the steady-state performance of the cell, are often neglected.

The objective of this study is, therefore, to investigate the effect of the two most common flow-field designs, namely, parallel and serpentine as representatives of diffusion-dominant and convection-enhanced flow-fields, respectively. A thorough understanding of how those two modes of species transport respond and the ability to identify which mode is favoured over the other under real automotive transient operations will help engineers to achieve better flow-field design.

This article is organised into 3 separate parts; the computational domain and model development together with boundary conditions and parameters used in the simulation are described in the first section which will then be followed by the results and discussions. The last section will give the readers conclusions drawn from this study and suggest further interesting and unsolved topics for the future work.

MODEL DEVELOPMENT

Computational Domain

Figure 1 shows the two flow-field designs; parallel (A) and single-serpentine (B). The current collectors are excluded from the study in order to reduce the cell count and hence computational cost. The domain therefore comprises of 7 layers, from top to bottom;

$$CH_{an}|GDL_{an}|Cl_{an}|PEM|CL_{ca}|GDL_{ca}|CH_{ca}$$

A side view of the cell is also given to illustrate how each layer is assembled to form a single cell (not to scale). The active areas of both cells are approximately 4 cm^2, the exact geometrical values are tabulated in **Table 1**.

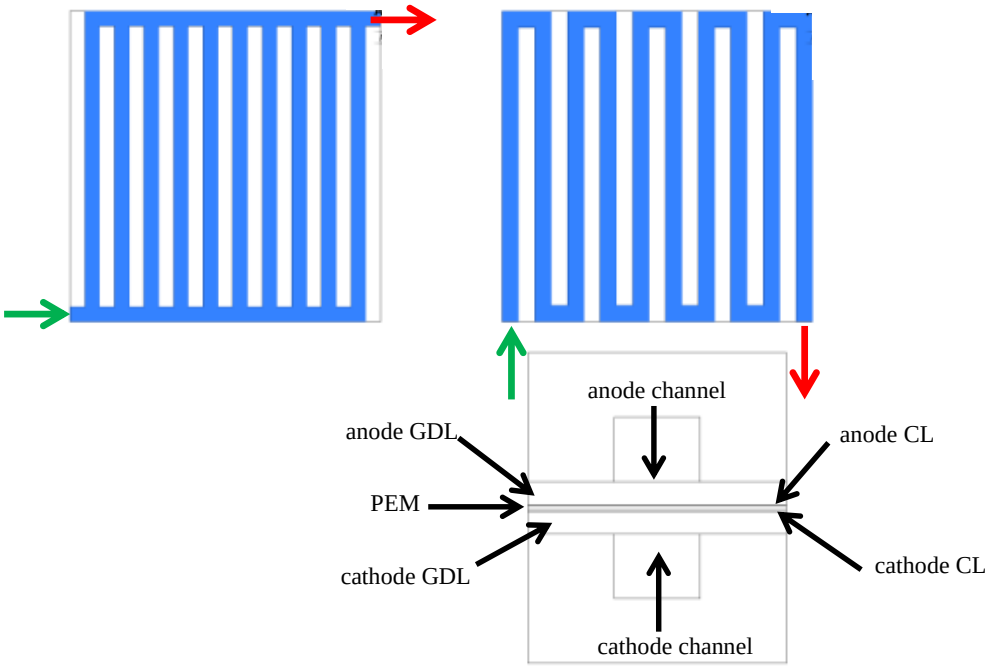

Figure 1: Parallel (A) and serpentine (B) designs; Green – Inlet, Red – Outlet

Table 1: Cell dimensions

Parameter	A	B
Cell width [mm]	21	19
Cell length [mm]	21	19
Channel width [mm]	1	1
Channel height [mm]	1	1
Rib width [mm]	1	1
GDL (Toray 120) thickness [μm]	370	370
CL thickness [μm]	20	20
PEM (Nafion 117) thickness [μm]	178	178
Active surface area [cm^2]	4.41	3.61

Modelling Assumptions

1. Incompressible and laminar flow throughout the domain at any operating conditions
2. The flow is fully developed at the outlet
3. The anode gas comprises of hydrogen and water vapour while the cathode gas is air (a mixture of oxygen, nitrogen, and water vapour). All gases are behaving as ideal gases.
4. Two-phase flow is treated throughout the domain; channels, GDLs, CLs, except membrane. Water is present in both form as liquid or vapour depending on the local saturation value.
5. The GDLs, CLs, and membrane are isotropic and homogenous.
6. The membrane is impermeable to reactant gases to neglect the gas cross-over
7. Constant and uniform potential at the two terminals due to very high electrical conductivity imposed.
8. The model is non-isothermal and hence all thermal properties of the flow are dependent on the local temperature

Governing Equations

A PEM fuel cell can be treated as an electrochemical system involving mass transport of reactant gas species, transport of electron, and heat transfer. Using a single-domain approach, the transport of each variable in all sub-domains can be written in a generic form of diffusive-convective transport equation. The source term, however, is treated specifically depending on the reaction in that particular sub-domain. The governing equations are only briefly given here of brevity, more details on the governing equations can be found elsewhere [22, 30]. The three-dimensional, multi-species, non-isothermal, and two-phase governing equations are given as, in vector forms;

1. Conservation of Mass

$$\varepsilon \frac{\partial \rho}{\partial t} + \nabla \cdot \left(\rho \vec{V}\right) = S_m \qquad (1)$$

At anode CL; $S_m = S_{H_2}$ (2)

At cathode CL; $S_m = S_{O_2} + S_{H_2O}$ (3)

Where $$S_{H_2} = -\frac{M_{H_2}}{2F} R_{an} \quad (4)$$

$$S_{O_2} = -\frac{M_{O_2}}{4F} R_{ca} \quad (5)$$

$$S_{cw} = \frac{M_{H_2O}}{2F} R_{ca} \quad (6)$$

2. Conservation of Momentum

$$\frac{1}{\varepsilon}\frac{\partial\left(\rho\vec{V}\right)}{\partial t} + \frac{1}{\varepsilon^2}\nabla\cdot\left(\rho\vec{V}\vec{V}\right) = -\nabla p + \nabla\bar{\bar{\tau}} + S_{p\vec{j}} \quad (7)$$

Where $\vec{j}$ represents *x*-, *y*-, and *z*-coordinates

$$S_{px} = -\frac{\mu}{\beta}u\ ,\ S_{py} = -\frac{\mu}{\beta}v\ ,\ S_{pz} = -\frac{\mu}{\beta}w \quad (8a\text{-}8c)$$

3. Conservation of Species

$$\varepsilon\frac{\partial\left(\rho x_i\right)}{\partial t} + \nabla\cdot\left(\rho x_i\vec{V}\right) = \nabla J_{\vec{j},i} + S_i \quad (9)$$

4. Conservation of energy

$$\begin{aligned}\varepsilon\frac{\partial\left(\rho h_0\right)}{\partial t} + \nabla\cdot\left(\rho h_0\vec{V}\right) &= \nabla\cdot\left(k\nabla T\right) + \frac{\partial\left(u\tau_{xx}\right)}{\partial x} + \frac{\partial\left(u\tau_{yx}\right)}{\partial y} + \frac{\partial\left(u\tau_{zx}\right)}{\partial z} \\ &+ \frac{\partial\left(v\tau_{xy}\right)}{\partial x} + \frac{\partial\left(v\tau_{yy}\right)}{\partial y} + \frac{\partial\left(v\tau_{zy}\right)}{\partial z} + \frac{\partial\left(w\tau_{xz}\right)}{\partial x} + \frac{\partial\left(w\tau_{yz}\right)}{\partial y} + \frac{\partial\left(w\tau_{zz}\right)}{\partial z} + S_h\end{aligned} \quad (10)$$

$$S_h = h_{react} - R_{an,ca}\eta_{an,ca} + I^2R_{Ohm} + h_L \quad (11)$$

5. Conservation of charge

$$\frac{\partial\rho_0}{\partial t} + \nabla\cdot\left(\sigma_{sol}\nabla\varphi_{sol}\right) + R_{sol} = 0 \quad (12)$$

$$\frac{\partial\rho_0}{\partial t} + \nabla\cdot\left(\sigma_{mem}\nabla\varphi_{mem}\right) + R_{mem} = 0 \quad (13)$$

Where ρ_0 is a local charge density which has a unit of Cm^{-3}

The source terms represent the transfer currents within the catalyst layers and are expressed by Butler-Volmer Equation;

$$R_{an} = \left(\varsigma_{an}j_{an}^{ref}\right)\left(\frac{C_{H_2}}{C_{H_2,ref}}\right)^{\gamma_{an}}\left(e^{\frac{\alpha_{an}F\eta_{an}}{RT}} - e^{\frac{-\alpha_{ca}F\eta_{an}}{RT}}\right) \quad (14)$$

$$R_{ca} = \left(\varsigma_{ca}j_{ca}^{ref}\right)\left(\frac{C_{O_2}}{C_{O_2,ref}}\right)^{\gamma_{ca}}\left(-e^{\frac{\alpha_{an}F\eta_{ca}}{RT}} + e^{\frac{-\alpha_{ca}F\eta_{ca}}{RT}}\right) \quad (15)$$

Mesh Generation

A hexahedral conformal mesh was chosen due to an orthogonal structure of the cell geometry and the mesh was made finer in the areas where there exists a high gradient of the variables of interest such as at the bends or the interface between the flow channels and GDLs. The number of cells of the resulting meshes are 449,664 and 387,328 for parallel (A) and serpentine (B) cells, respectively. This gave a good balance between accuracy, computational time, and good convergence due to minimal cell counts and zero cell skewness and the mesh B is shown in **Figure 2**.

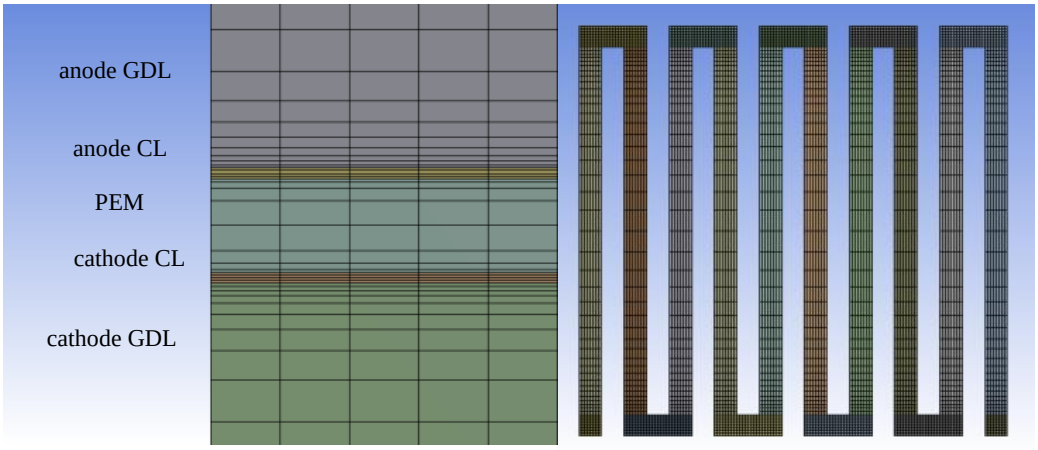

Figure 2: Side and top views of mesh used (serpentine only)

Boundary and Operating Conditions

Figure 3 shows the locations where different types of boundary conditions are applied as follows:

i. Inlets: velocity inlet (u_{an}, u_{ca}), mass fraction of species (H_2, H_2O at anode and O_2, H_2O at cathode), and gas temperature (T_{in})
ii. Outlets: pressure outlet
iii. Cell side walls and flow channel walls: No slip condition and fixed temperature at the operating temperature. The small computational domain can effectively have relatively uniform temperature throughout.
iv. GDL surfaces (wall terminals): Potentiostatic boundary condition is applied; a constant value for steady-state simulation and varying during transient simulation.

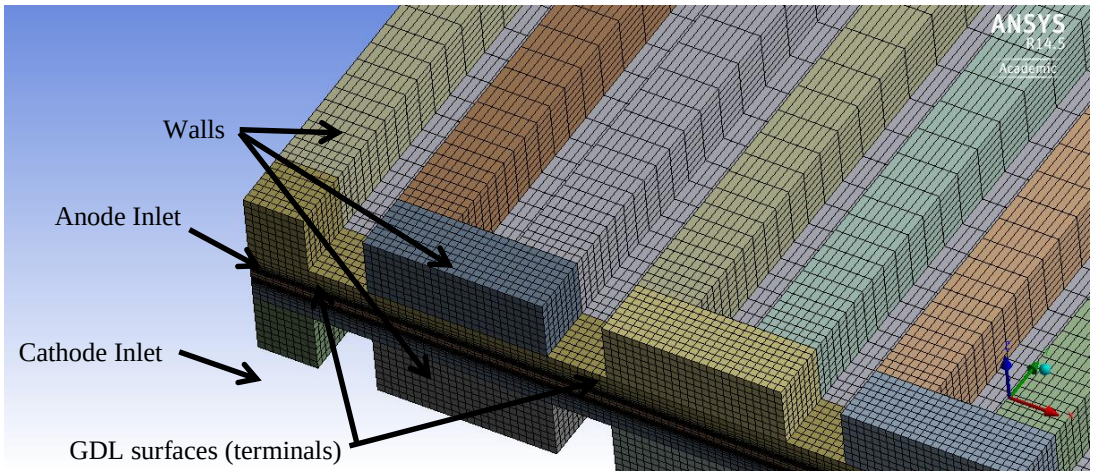

Figure 3: Boundary conditions and locations where they are applied

In a transportation application, carrying an on-board humidifier might not be practical in the system design perspective and therefore achieving good hydration of the cathode-side membrane by the produced water (self-humidification) is favourable. The "dry" condition where the reduced relative humidity of 50% for both anode and cathode (typical relative humidity of ambient air) gases was investigated as opposed to the fully-humidified or "wet"

condition ($RH\%_{an} = RH\%_{ca} = 100\%$). This resulted in different composition of each species in the reactant gases between the two dry and wet conditions. **Tables 2** and **3** summarise the boundary and operating conditions used in the simulation.

Table 2: Modelling parameters

Anode exchange current density [32]	80	Am^{-2}
Cathode exchange current density [32]	2×10^{-4}	Am^{-2}
H_2 reference molar concentration [32]	40.88	$molm^{-3}$
O_2 reference molar concentration [32]	40.88	$molm^{-3}$
Anode concentration exponent [31]	0.5	-
Cathode concentration exponent [31]	1	-
Anode charge transfer coefficient [31]	1	-
Cathode charge transfer coefficient [31]	1	-
H_2 reference diffusivity [31]	8×10^{-5}	m^2s^{-1}
O_2 reference diffusivity [31]	2×10^{-5}	m^2s^{-1}
H_2O reference diffusivity [31]	5×10^{-5}	m^2s^{-1}
Anode/cathode GDLs porosity [typical value]	0.5	-
Anode/cathode GDLs viscous resistance [32]	8.93×10^{13}	m^{-2}
Anode/cathode GDLs contact angle [31]	30	Degree
Anode/cathode CLs porosity [31]	0.82	-
Anode/cathode CLs viscous resistance [32]	8.93×10^{13}	m^{-2}
Anode/cathode CLs contact angle [31]	30	degree
Anode/cathode specific surface active area [31]	1.25×10^{7}	m^{-1}
Membrane equivalent weight [33]	1100	$kgkmol^{-1}$
Membrane protonic conduction coefficient [33]	1	-
Membrane protonic conduction exponent [33]	1	-
Saturation exponent for pore blockage [31]	2	-
GDLs/CLs thermal conductivity [typical value]	2	$Wm^{-1}K^{-1}$
GDLs/CLs electrical conductivity [typical value]	300	Sm^{-1}

Table 3: Operating conditions

Parameter		**A**	**B**
"Wet" $100\%RH_{an,\ ca}$	Anode inlet velocity at 353.15 K [ms^{-1}]	2.16	1.77
	Cathode inlet velocity at 353.15 K [ms^{-1}]	3.09	2.53
	Mole fraction of H_2/H_20 at anode	0.767/0.233	
	Mole fraction of O_2/H_2O at cathode	0.161/0.233	
	Anode terminal potential [V]	0	
	Open-circuit voltage [V]	1.181	
"Dry" $50\%RH_{an,\ ca}$	Anode inlet velocity at 353.15 K [ms^{-1}]	1.87	1.53
	Cathode inlet velocity at 353.15 K [ms^{-1}]	2.68	2.19
	Mole fraction of H_2/H_20 at anode	0.883/0.117	
	Mole fraction of O_2/H_2O at cathode	0.185/0.117	
	Anode terminal potential [V]	0	
	Open-circuit voltage [V]	1.184	
Anode/cathode stoichiometry		5/3	
Operating pressure [Pa]		202650	
Operating temperature [K]		353.15	

RESULTS AND DISCUSSION

Model Validation

The validity of the proposed model was examined by comparing the numerical results to the experimental data published by Mench et al. [34]. From **Figure 4**, it can be seen that the predictions agree very well with the experimental data not only within the activation and Ohmic regions but also in the mass transport limit region.

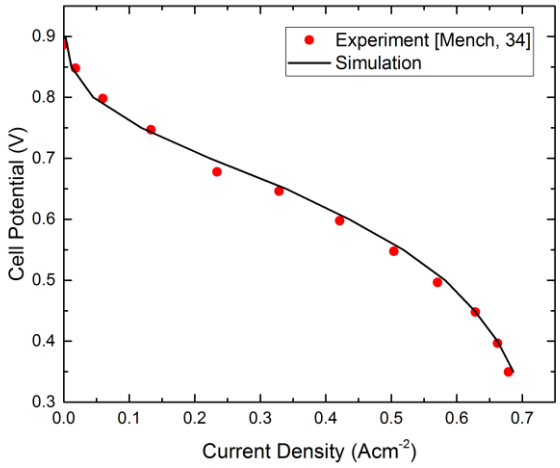

Figure 4: Model validation

Steady-state Performance

When a current is drawn from the cell, it is always associated with three losses; activation, Ohmic, and concentration loss, which occur mutually but dominate over different regions on the curve results in a deviation of the cell potential from the equilibrium voltage (open circuit voltage). The more current is drawn, the lower the cell potential. The cell is said to be polarised, and hence the name of the poralisation curve which is commonly used as the general indicator of the steady-state performance of a PEM fuel cell as shown in **Figure 5** for both cells under wet and dry conditions.

Clearly, comparing the poralisation curve of each cell under wet and dry conditions, both cells benefit from fully humidified anode and cathode gases that gave better membrane hydration which in turn resulted in higher protonic conductivity and current density.

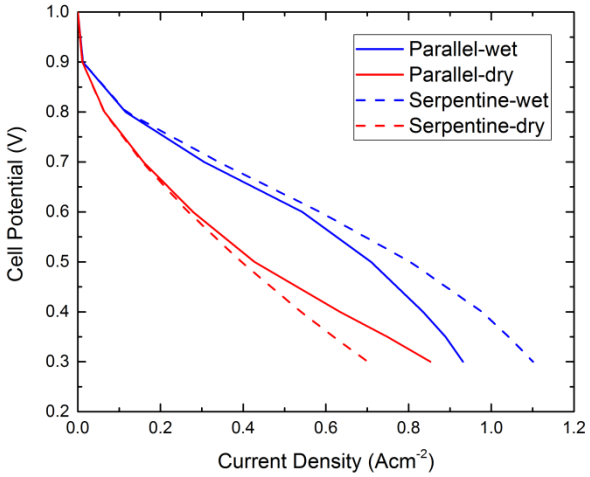

Figure 5: Polarisation curves of both cells under wet and dry conditions

Interestingly, the parallel flow-field outperformed the serpentine flow-field under the dry condition. The two polarisation curves under dry reactant gases do not exhibit an abrupt drop of the current density when the cell is operated at low voltage below 0.40 V. This region is known as the mass-transport limit region where the fluxes of reactant species to the reaction sites cannot catch up with the fast reaction kinetics as they are impeded or completely blocked by product water and this manifest itself as a sharp drop in the cell voltage at high current density. It should be noted that a small cell active area and dry inlet gases used result in an overly effective species distribution and product water removal and hence no flooding occurs. As a consequence, unlike larger commercial-sized cells, the two corresponding cases did not suffer from mass-transport limit and only suffered from Ohmic loss down to the final operating voltage of 0.30 V.

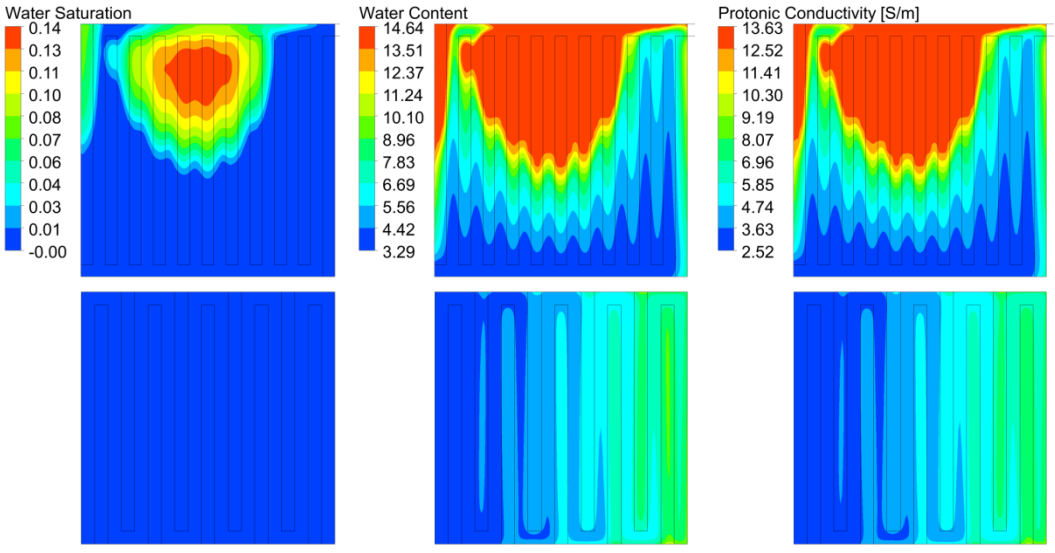

Figure 6: Water saturation, membrane water content, and protonic conductivity of cells A (top) and B (bottom) under dry condition and at cell potential of 0.30 V

The parallel cell started to outperform the serpentine cell at the operating voltage of 0.60 V and the difference increased further as the cell potential was lowered. This is the result of a convective-dominant nature of the serpentine flow-field that can better remove water out of the channels and GDLs which effects the membrane hydration. This adverse effect is more pronounced under a dry condition when there is not sufficient water to keep the membrane well-hydrated and causes membrane dry-out and low protonic conductivity as confirmed by **Figure 6** which shows the water saturation, membrane water content, and protonic conductivity at the interface between cathode catalyst layer and membrane at the operating voltage of 0.30 V. In an extreme case, it can permanently damage the membrane and hence should be avoided.

Under the wet condition which is often regarded as standard operating condition for all PEM fuel cell modelling, the serpentine cell outperformed its parallel counterpart especially at the mass transfer limit region. It is clear that at higher operating current, excessive water both from the humidified gases and electrochemical reaction can cause GDL flooding and prevent the reactant species from reaching the reaction sites while the serpentine flow-field gives better water removal and promotes higher reactant species concentration at the catalyst sites and hence higher current density.

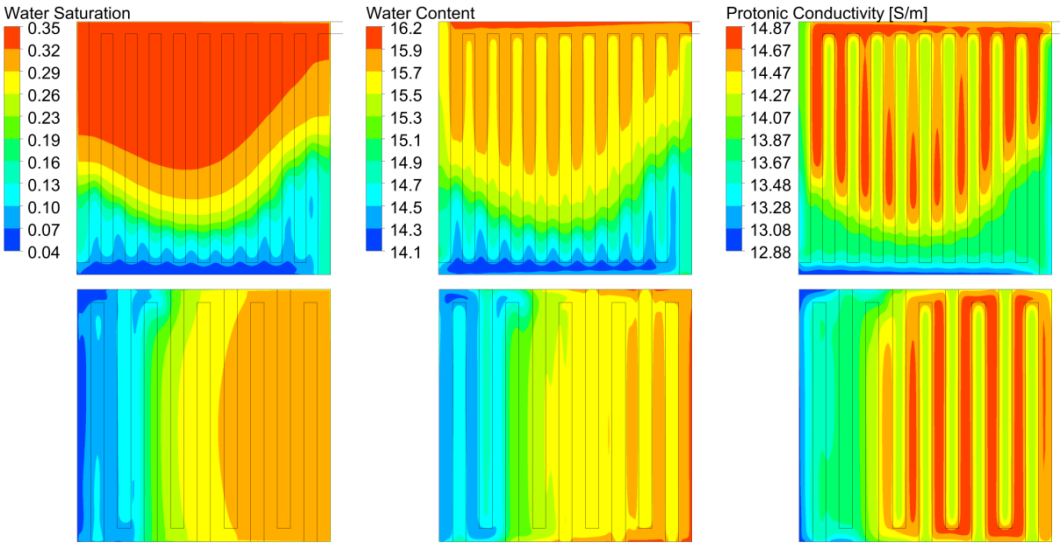

Figure 7: Water saturation, membrane water content, and protonic conductivity of cells A (top) and B (bottom) under wet condition and at cell potential of 0.30 V

The distributions of water saturation, membrane water content, and protonic conductivity on the interface of cathode catalyst layer and membrane are shown in **Figure 7** and suggests that the parallel cell should perform better due to higher protonic conductivity. Since Cell A has a slightly better-hydrated membrane but lower current density, this suggests that it suffered from oxygen transport and instead of looking at the oxygen mass fraction contour which can be misleading as discussed in the previous work [22], a closer look at the reaction heat source on the interface between cathode catalyst layer and membrane at operating voltage of 0.30 V will indicate the exact location and absolute quantity of the oxygen being consumed. **Figure 8** reveals that though Cell A has higher membrane water content and protonic conductivity due to presence of more water in the domain, this excessive water has a negative effect on the cell

in which it blocks oxygen molecules from diffusing into the reaction site and therefore less oxygen could diffuse into the reaction site and take part in the reaction. The heat of reaction is lower in Cell A especially the areas with high water saturation value which indicates the GDL flooding.

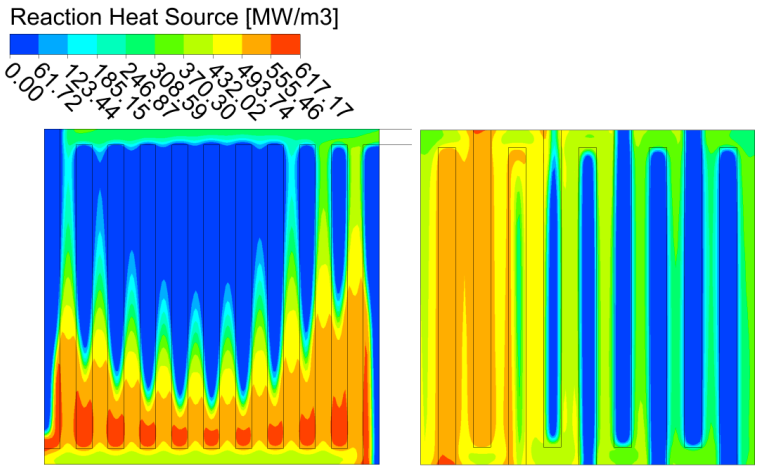

Figure 8: Reaction heat source of cells A (left) and B (right) under wet condition and at cell potential of 0.30 V

The pressure contours between cathode inlet and outlet of each cell at 0.30 V operating voltage for the wet conditions are shown in **Figure 9**. Obviously, due to a long and meandering channel with many bends of Cell B, the pressure drop is slightly higher than that of Cell A. However, in larger cells where the channel length will increase considerably and more bends, the pressure drop of a serpentine flow-field type is expected to be much higher than its parallel counterpart and this high pressure drop will be more pronounced in a PEM fuel cell where more than one hundred cells are stacked up. In a system design perspective involving large cell active area or a number of cells in a stack, this pressure drop characteristic should not be overlooked.

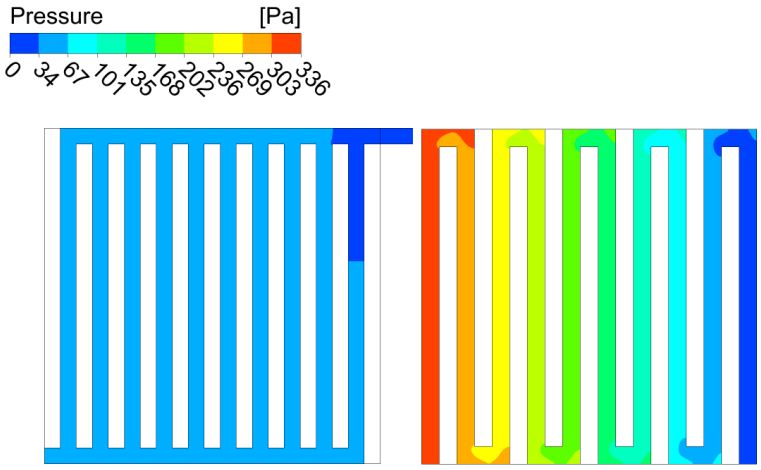

Figure 9: Pressure field in the cathode channel of cells A (left) and B (right) under wet condition and at cell potential of 0.30 V

Transient Response to Step Change in Voltage

The voltage step-up and step-down were used to represent the situations when the engine is subjected to a sudden change in power demand such as engine shut-down and engine start-up, respectively. The cell potential change between 0.80 and 0.50 V was chosen as this is the typical range of the cell potential in operation. In order to make the discussion easy to follow, all 8 conditions are labelled as shown in **Table 4**.

Table 4: List of cases with its description

Case Number	Flow-field Type	Humidity Condition	Voltage Change Type (step change)
1	Parallel	Wet	0.80 → 0.50
2	Parallel	Dry	0.80 → 0.50
3	Serpentine	Wet	0.80 → 0.50
4	Serpentine	Dry	0.80 → 0.50
5	Parallel	Wet	0.50 → 0.80
6	Parallel	Dry	0.50 → 0.80
7	Serpentine	Wet	0.50 → 0.80
8	Serpentine	Dry	0.50 → 0.80

The current responses to voltage step-down for both cells under wet and dry conditions for Cases 1-4 are given in **Figure 10**. It should be noted that due to different initial and final current densities of each case, in order to give a fair comparison between these cases, the equilibrium current density at cell potential of 0.30 V of each cell was used to normalise the current response, these are 0.709566, 0.427582, 0.803884, and 0.3955 Acm^{-2} for Cases 1-4, respectively.

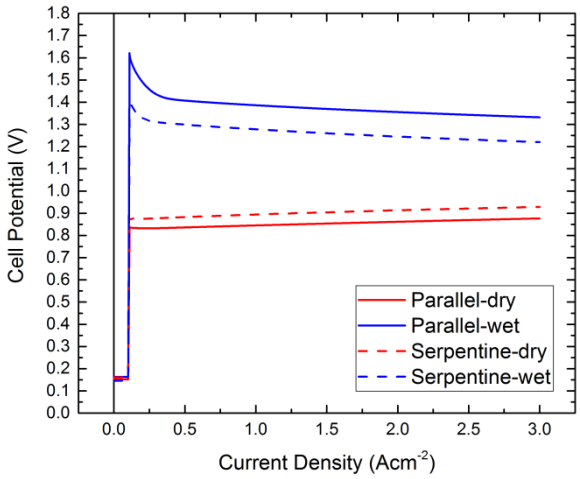

Figure 10: Current responses to voltage step down for Cases 1-4

The initial operating voltage was maintained at 0.80 V before it was stepped down to 0.50 V at t = 0.10 second followed by an immediate response of the current before they gradually approached the final value as the cell continued to adjust itself to the new equilibrium state. This sharp rise or a peak of current density is regarded as a current overshoot. However, there exists the discrepancy in the behaviours of the cells under wet and dry conditions in which the

wet cells (Case 1 and 3) showed some degree of current overshoot and constantly approached the new value from the top side while the dry cells (Cases 2 and 4), however, show the sharp rise in current density up to a certain point before gradually reaching the equilibrium value from the bottom side without any current overshoot. The current overshoot in Cases 1 and 3 is the result of an already available oxygen reservoir at the cathode reaction site. At the time t < 0.10 second when the cell potential is at 0.80 V and the rate of electrochemical reaction is low, oxygen which has diffused through the GDL to the reaction site is consumed only partially. When the cell potential was reduced to 0.50 V at the time t = 0.10 second, the reaction rate was increased immediately and the already available oxygen was consumed in the reaction almost limitlessly over the entire active area. The combination of almost unlimited oxygen reservoir in the catalyst layer and a well-hydrated membrane resulted manifested itself as current overshoot. After the time t = 0.12 second, the available oxygen started to decrease because oxygen diffusion could not catch up with the increased oxygen consumption rate especially at the outlet area and this gave a gradual drop in current density until it reached the new steady-state where the rates of oxygen consumption and diffusion were in equilibrium.

The higher reaction rate in the dry cases, on the other hand, caused a sharp rise of current density up to a point where it could not increase further without current overshoot even there is excessive oxygen as in the wet conditions because it was restricted by the low protonic conductivity of a dry membrane. As the time progressed, the higher water production rate continued to hydrate the membrane and increase protonic conductivity and its effect can be seen from a gradual increase in current density.

In a dynamic performance perspective, the wet cells responded to the step change in voltage with prohibitively high current overshoot which are 60% and 40% greater than the desired value for Cases 1 and 3, respectively. An excessively high current density will result in local hotspot and thermal stress which can membrane permanent damage in an extreme case. The dry cells, despite of not being able to meet the desired current, do not cause current overshoot that can damage the membrane and it suggests that if the simulation was run further, they will reach the new current value before the wet cells and it is said to response quicker.

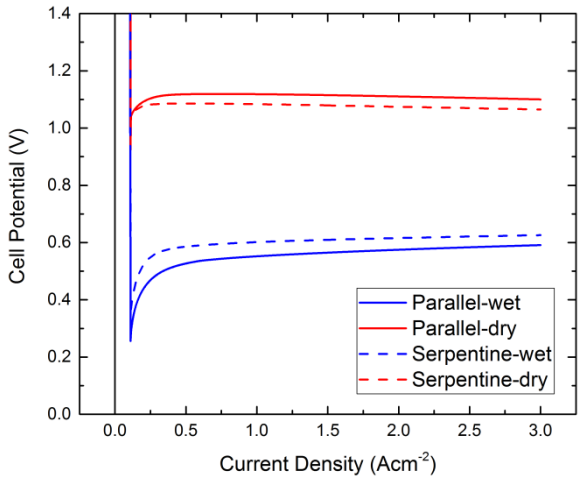

Figure 11: Current responses to voltage step down for Cases 5-8

The current response to a voltage step-up for Cases 5-8 are now presented in **Figure 11**. Similarly, all cases exhibited a current undershoot immediately after the voltage was stepped up followed by a period where the current reached the new equilibrium value. The current undershoot is a result of the non-uniformity of the oxygen distribution over the active surface similar to that causes the current overshoot. At time $t < 0.10$ second where the reaction and oxygen consumption rate were high, the oxygen available is highly non-uniform, being highest near the inlet and almost depleted at the outlet region. When the voltage was stepped up at the time $t = 0.10$ second, according to the lower reaction rate, the oxygen consumption rate was reduced throughout the active surface resulting in current undershoot due to very limited oxygen at the active site. The cells required some time for fresh oxygen to diffuse to the active site from the channel to reach the new equilibrium state and hence a gradual increase in current for Cases 5 and 7. For the dry Cases 6 and 8, the secondary current response was observed that is the current first undershot followed by a slight current overshoot before it constantly approached the final value as opposed to Cases 5 and 7 where the currents undershot and approached the final values. This can be described by the combined influence of membrane water content and the dry operating condition. The current undershoot was caused by the immediate reduction of oxygen consumption rate and hence less current was generated. As the cell continued to adjust to the new equilibrium, the replenishment of fresh oxygen by diffusion was considerably faster the transport of membrane water content and hence the membrane water content and protonic conductivity were still high from the previous low cell potential operation, the current density therefore exceeded the new value due to a better hydrated membrane. As time progressed, however, the membrane started to lose its hydration through the membrane water desorption to adjust to the new equilibrium and this resulted in a gradual decrease in current.

In a dynamic performance perspective, the dry cells are superior to wet cells both in terms of undershoot magnitude and time taken to reach the new steady-state value. The deviation of the current from the final value falls within 10% for the dry cases whereas the current can be significantly lower (as high as 80%) than the desired value for the wet cases which is not a good response. This is due to the fact that the wet cells were operating under a high humidity condition and hence the flooding of GDL will prevent fresh oxygen from the channel to replenish the active site and this caused the current undershoot to be more severe than the dry cells where oxygen diffusion was not impeded.

CONCLUSION

A three-dimensional, multi-species, and multi-phase PEM fuel cell model was developed in order to investigate the effect of flow-field geometries on both steady-state and transient performances. It is found that the membrane water content is the key parameter in determining the successful operation of a PEM fuel cell in which it control the protonic conductivity of the cell which in turn effects the output current density in the steady-state operation and the current response profile in the transient operation. This confirms that water management in the cell is very important and it is found to be strongly coupled to the flow-field design. A good flow-field design that promotes good species transport and effective water removal will guarantee a better PEM fuel cell.

In a steady-state run, the convection-dominant flow induced by a serpentine flow-field proves to be more effective than a diffusion-dominant flow of the parallel flow-field in terms of better species concentration at the reactive site and superior product water removal from the cell. However, when the net power is considered, a higher pressure drop along the channel of the serpentine design should not be ignored especially when the PEM fuel cell stack comprising over a hundred full-scale cells is considered. However, when the cell is to be operated under dry reactant gases, the superior water removal ability of the serpentine flow-field will adversely affect the protonic conductivity of the membrane and the current will be decreased. In a transient operation, on the other hand, the combination of dry operating condition and serpentine flow-field will outperform the parallel design due to fast water removal out of the porous layers which allows for fast oxygen replenishment to the active site without being impeded by excessive water.

In a real automotive operation, the cell is subjected to various voltage change patterns at different operating voltages and different magnitudes and the relationship of the flow-field geometries to these various voltage changes remains as a question of the future work.

References

[1] Wang Y., Chen K S., Mishler J., Cho S C., Adroher X C., A review of polymer electrolyte membrane fuel cells: Technology, applications, and needs on fundamental research, Applied Energy, Vol. 88, No. 4, 2011, pp. 981-1007.

[2] Springer T.E., Zawodzinski T.A., and Gottesfeld S., *Polymer electrolyte fuel cell model*, Journal of The Electrochemical Society, Vol. 138, No. 8, August 1991, pp. 2334-2342

[3] Bernadi D.M. and Verbrugge M., *A mathematical model of solid-polymer-electrolyte fuel cell*, Journal of The Electrochemical Society, Vol. 139, No. 9, September 1992, pp. 2477-2491

[4] Bernadi D.M. and Verbrugge M., *Mathematical model of a gas diffusion electrode bonded to a polymer electrolyte*, AlChE Journal, Vol. 37, No. 8, August 1911, pp. 1151-1163

[5] Gurau V., Liu H., and Kakac S., *Two-dimensional model for proton exchange membrane fuel cells*, AlChE Journal, Vol. 44, 1998, pp. 2410-2422

[6] Wang CY, Gu W.B., and Liaw B.Y., *Micro-macroscopic coupled modelling of batteries and fuel cells*, Journal of The Electrochemical Society, Vol. 145, 1998, pp. 3407-3417

[7] Zhou T. and Liu H., *A general three-dimensional model for proton exchange membrane fuel cells*, International Journal of Transport Phenomena, Vol. 3, No. 3, 2001, pp. 177-198

[8] Wang X.D., Duan Y.Y., Yan W.M., and Peng X.F., *Effects of flow channel geometry on cell performance for PEM fuel cells with parallel and interdigitated flow fields*, Electrochimica Acta, Vol. 53, 2008, pp. 5334-5343

[9] Yan W.M., Liu H.C., Soong C.Y., Chen F., and Cheng C.H., *Numerical study on cell performance and local transport phenomena of PEM fuel cells with novel flow field designs*, Journal of Power Sources, Vol. 161, 2006, pp. 907-919

[10] Jeon D.H., Greenway S., Shimpalee S., and Van Zee J.W., *The effect of serpentine flow-field designs on PEM fuel cell performance*, International Journal of Hydrogen Energy, Vol. 33, 2008, pp. 1052-1066

[11] Shimpalee S. and Van Zee J.W., *Numerical studies on rib & cannel dimensión of flow-field on PEMFC performance*, International Journal of Hydrogen Energy, Vol. 32, 2007, pp. 842-856

[12] Wang X.D., Duan Y.Y., Yan W.M., and Peng X.F., *Local transport phenomena and cell performance of PEM fuel cells with various serpentine flow field designs*, Journal of Power Sources, Vol. 175, 2008, pp. 397-407

[13] Dawes J.E., Hanspal N.S., Family O.A., and Turan A., *Three-dimensional CFD modelling of PEM fuel cells: An investigation into the effects of water flooding*, Chemical Engineering Science, Vol. 64, 2009, pp. 2781-2794

[14] Nguyen P.T., Berning T., and Djilali N., *Computational model of a PEM fuel cell with serpentine gas flow channels*, Journal of Power Sources, Vol. 130, 2004. Pp. 149-157

[15] Kumar A. and Reddy R.G., *Effect of channel dimensions and shape in the flow-field distributor on the performance of polymer electrolyte membrane fuel cells*, Journal of Power Sources, Vol. 113, 2003, pp. 11-18

[16] Wang X.D., Duan Y.Y., and Yan W.M., *Novel serpentine-baffle flow field design for proton exchange membrane fuel cells*, Journal of Power Sources, Vol. 173, 2007, pp. 210-221

[17] Roshandel R., Arbabi F., and Moghaddam G.K., *Simulation of an innovative flow-field design based on a bio inspired pattern for PEM fuel cells*, Renewable Energy, Vol. 41, 2012, pp. 86-95

[18] Hashemi F., Rowshanzamir S., and Rezakazemi M., *CFD simulation of PEM fuel cell performance: Effect of straight and serpentine flow fields*, Mathematical and Computer Modelling, Vol. 55, 2012, pp. 1540-1557

[19] Siegel N.P., Ellis M.W., Nelson D.J., and Von Spakovsky M.R., *A two-dimensional computational model of a PEMFC with liquid water transport*, Journal of Power Sources, Vol. 128, 2004, pp. 173-184

[20] Choopanya P. and Peng Z., *An investigation on steady-state performance of conventional and serpentine flow-fields for automotive polymer electrolyte membrane fuel cell*, SCODECE Internal Conference/International Forum on Vehicle Control, 2012

[21] Peng Z. and Choopanya P., *CFD investigation into internal flows of PEM fuel cell for optimal performances*, Advanced Materials Research, Vol. 724-725, 2013, pp. 757-761

[22] Choopanya P. and Yang Z., *Transient performance investigation of different flow-field designs of automotive polymer electrolyte membrane fuel cell (PEMFC) using computational fluid dynamics (CFD)*, Proceedings of the 10th International Conference on Heat Transfer, Fluid Mechanics, and Thermodynamics, 14-16 July 2014, pp. 583-592.

[23] Hogarth W.H.J. and Benziger J.B., *Dynamics of autohumidified PEM fuel cell operation*, Journal of The Electrochemical Society, Vol. 153, 2006, pp. A2139-A2146

[24] Yan Q., Toghiani H., and Causey H., *Steady state and dynamic performance of proton exchange membrane fuel cells (PEMFCs) under various operating conditions and load changes*, Journal of Power Sources, Vol. 161, 2006, pp. 492-502

[25] Adcock P., Keels A., and Jackson C., *PEM fuel cells for road vehicles*, EET-2208 European Ele-Drive Conference, International Advanced Mobility Forum, Geneve, Switzerland, March 11-13, 2008

[26] Andreassi L., Cordiner S., and Romanelli F., *Performances analysis of PEM fuel cell based automotive systems under transient conditions*, SAE Technical Paper 2003-01-1144, 2003, pp. 245-258

[27] Pathapati P.R., Xue X., and Tang J., *A new dynamic model for predicting transient phenomena in a PEM fuel cell system*, Renewable Energy, Vol. 30, 2005, pp. 1-22

[28] Pasricha S. and Shaw S.R., *A dynamic PEM fuel cell model*, IEEE Transactions on Energy Conversion, Vol.21, No. 2, June 2006, pp. 484-490

[29] Srinivasa Raju P., Prasada Raju P.V.V.N.R., Sharma K.V., and Raju B.J.J., *Dynamic modeling of a PEM fuel cell*, European Journal of Scientific Research, Vol. 43, No. 1, 2010, pp. 138-147

[30] Wang Y. and Wang Y.C., Modeling polymer electrolyte fuel cells with large density and velocity changes, Journal of The Electrochemical Society, Vol. 152, No. 2, pp. A445-A453.

[31] Iranzo A., Munoz M., Rosa F., and Pino J., *Numerical model for the performance prediction of a PEM fuel cell cell. Model results and experimental validation*, International Journal of Hydrogen Energy, Vol. 35, 2010, pp. 11533-11550

[32] Ju H. and Wang C.Y., *Experimental validation of a PEM fuel cell model by current distribution data*, Journal of The Electrochemical Society, Vol. 151, 2004, pp. A1954-A1960

[33] *PEMFC and Electrolyte Add-on Module User Guide*, Release 12.0, ANSYS Inc., January 23, 2009

[34] Mench M.M., Wang C.Y., and Ishikawa M., *In situ current distribution measurements in polymer electrolyte fuel cells*, Journal of The Electrochemical Society, Vol. 150, 2003, pp. A1052-A1059